(Supplementary Materials) Non-Normal Phase Transitions: A New Universality in Complex Systems

Virgile Troude and Didier Sornette
Institute of Risk Analysis, Prediction and Management (Risks-X), Academy for Advanced Interdisciplinary Sciences, Southern University of Science and Technology, Shenzhen, China

We first introduce the mathematical framework and key concepts used throughout the Supplementary Material (SM). We provide the necessary background and definitions for understanding the derivations and analysis presented in the subsequent sections.

This Supplementary Material aims to present analytical derivations demonstrating how non-normality impacts the probability of transitions between states in non-variational systems. The main results show that non-normality leads to an amplification mechanism, enabling faster transitions between states and even causing systems to exit stable equilibrium more rapidly due to this amplification.

CONTENTS

I. MATHEMATICAL FRAMEWORK

In this appendix, we provide the mathematical background and assumptions underlying our analysis. We first introduce the dynamical system of interest, before reformulating the problem in the language of stochastic calculus.

A. Generalized Langevin System

We consider an overdamped Langevin dynamics describing the evolution of an N-dimensional state vector $\mathbf{x}$, subject to a generalized force $\mathbf{f}$ and stochastic fluctuations

$$\dot{\mathbf{x}} = \mathbf{f}(\mathbf{x}) + \sqrt{2\delta}\,\boldsymbol{\eta}, \qquad \boldsymbol{\eta} \overset{\text{iid}}{\sim} \mathcal{N}(0, \mathbf{I}), \tag{1}$$

where δ denotes the noise amplitude. In physical systems where the noise originates from thermal fluctuations, one has $\delta = k_B T$, with k_B Boltzmann's constant and T the temperature.

By Hodge decomposition—a generalization of the Helmholtz decomposition to higher dimensions [1, 2] – the generalized force can be expressed as

$$f_i(\mathbf{x}) = -\partial_i \phi(\mathbf{x}) + \sum_j \partial_j A_{ij}(\mathbf{x}), \tag{2}$$

where $\phi(\mathbf{x})$ is a scalar potential and $\mathbf{A}(\mathbf{x})$ is an anti-symmetric (anti-Hermitian in the complex case) matrix. The first term represents a conservative (*longitudinal*) force, while the second corresponds to a non-conservative (*transversal*) force. Systems of this type are called *non-variational*, as they do not generally derive from a least-action principle.

Near a stable fixed point $\mathbf{x}_0$, the dynamics can be linearized as

$$\dot{\mathbf{x}} \approx \mathbf{J}_f(\mathbf{x}_0)\,\mathbf{x} + \sqrt{2\delta}\,\boldsymbol{\eta}, \tag{3}$$

where $\mathbf{J}_f(\mathbf{x}_0)$ is the Jacobian of $\mathbf{f}$ at $\mathbf{x}_0$. Stability requires that all eigenvalues of $\mathbf{J}_f(\mathbf{x}_0)$ have negative real parts.

If $\mathbf{A} = 0$ in (2), then the system is variational and $\mathbf{J}_f(\mathbf{x}_0)$ is Hermitian, i.e. $\mathbf{J}_f(\mathbf{x}_0) = \mathbf{J}_f(\mathbf{x}_0)^\dagger$. Our focus, however, is on *non-normal systems*, characterized by $[\mathbf{J}_f(\mathbf{x}_0), \mathbf{J}_f(\mathbf{x}_0)^\dagger] \neq 0$, which implies that $\mathbf{J}_f(\mathbf{x}_0)$ cannot be diagonalized in a unitary basis. Even when such systems are linearly stable, transient deviations may be strongly amplified, and this amplification grows with the degree of non-normality.

A natural quantitative measure of non-normality is the condition number κ of the eigenbasis transformation of $\mathbf{J}_f(\mathbf{x}_0)$ [3]. In this work, we investigate the leading-order behavior of escape probabilities in the asymptotic regime $\kappa \gg 1$.

B. Problem Statement

We now reformulate the problem using the framework of stochastic calculus. Let $(\Omega, \mathcal{F}, \mathbb{P})$ be a filtered probability space supporting an N-dimensional Brownian motion $\mathbf{W}$. We consider the Itô stochastic differential equation

$$d\mathbf{x} = \mathbf{f}(\mathbf{x})\,dt + \sqrt{2\delta}\,d\mathbf{W}, \qquad \mathbf{x} \in \mathbb{R}^N, \;\; 0 < \delta \ll 1, \tag{4}$$

where $\mathbf{f} \in C^2(\mathbb{R}^N; \mathbb{R}^N)$ is the drift function. We assume that $\mathbf{f}$ satisfies a sub-quadratic growth condition, ensuring the existence of global strong solutions. Equation (4) is equivalent to (1), but expressed in stochastic calculus notation.

We focus on two disjoint open subsets $A, B \subset \mathbb{R}^N$, each containing a hyperbolic equilibrium of $\mathbf{f}$: $\mathbf{a} \in A$ and $\mathbf{b} \in B$. The central object of interest is the transition probability

$$\mathcal{P}^\delta := \mathbb{P}^\delta_{\mathbf{a}}\{\tau_B < \tau_{\partial A}\}, \tag{5}$$

where the stopping times are defined by

$$\tau_B := \inf_{t>0}\{\mathbf{x}_t \in B\}, \qquad \tau_{\partial A} := \inf_{t>0}\{\mathbf{x}_t \notin A\}. \tag{6}$$

We are particularly interested in the small-noise limit $\delta \to 0^+$.

The main objective of this work is to quantify how strong non-normality of the Jacobian $\mathbf{J}(\mathbf{x}) := D\mathbf{f}(\mathbf{x})$ modifies the asymptotic behavior of $\mathcal{P}^\delta$.

C. Large-Deviation Framework

For any fixed time horizon $\tau > 0$, the law of the process $(\mathbf{x}_t)_{t\in[0,\tau]}$ satisfies a Large-Deviation Principle (LDP) on the space $C([0,\tau];\mathbb{R}^N)$, characterized by the good rate function (action functional)

$$S_\tau[\mathbf{x}] = \frac{1}{4}\int_0^\tau \left\|\dot{\mathbf{x}}_t - \mathbf{f}(\mathbf{x}_t)\right\|^2 dt, \qquad \mathbf{x} \in H^1([0,\tau];\mathbb{R}^N). \tag{7}$$

According to Freidlin–Wentzell theory, the transition probability admits the asymptotic representation

$$\mathcal{P}^\delta \asymp \exp\left(-\frac{S}{\delta}\right), \qquad S := \inf_{\tau>0} \inf_{\mathbf{x}(0)=\mathbf{a},\, \mathbf{x}(\tau)\in B} S_\tau[\mathbf{x}], \tag{8}$$

where S is the *quasi-potential* between the equilibrium $\mathbf{a}$ and the set B. The second $\inf_{\mathbf{x}(0)=\mathbf{a},\, \mathbf{x}(\tau)\in B}$ in (8) is taken over all paths starting from $\mathbf{x}(0)$ and ending in domain B.

To ensure the validity of the large-deviation approximation and the asymptotic expansions employed, we impose the following assumptions:

- **(A1) Smoothness:** The drift $\mathbf{f}$ is twice continuously differentiable ($\mathbf{f} \in C^2$) and satisfies a sub-quadratic growth bound, i.e. $\|\mathbf{f}(\mathbf{x})\| \le C(1 + \|\mathbf{x}\|)$.
- **(A2) Hyperbolicity:** The Jacobians $D\mathbf{f}(\mathbf{a})$ and $D\mathbf{f}(\mathbf{b})$ are hyperbolic, meaning that all their eigenvalues have strictly negative real parts.
- **(A3) Unique Minimizer:** The optimization problem in (8) admits a unique minimizing path $\mathbf{x}^*$.
- **(A4) Local Uniformity:** The asymptotic expansions derived later remain uniformly valid in the scaling parameter κ within a local neighborhood of interest.

Under **(A1)**–**(A3)**, the LDP and associated saddle-point approximations are rigorous. Assumption **(A4)** ensures uniformity in the large shear introduced by non-normality, as measured by κ.

Different approaches can be used to evaluate the quasi-potential S. One possibility is to identify the *instanton* path by minimizing the Lagrangian

$$L(\dot{\mathbf{x}}, \mathbf{x}) := \tfrac{1}{4}\left\|\dot{\mathbf{x}} - \mathbf{f}(\mathbf{x})\right\|^2, \tag{9}$$

which leads to the Euler–Lagrange equation

$$\frac{d}{dt}\frac{\partial L}{\partial \dot{\mathbf{x}}} = \frac{\partial L}{\partial \mathbf{x}}. \tag{10}$$

Alternatively, and more conveniently for our analysis, one may adopt the Hamilton–Jacobi formalism. Assuming the minimizing action can be represented as a scalar field $S(\mathbf{x})$, for each infinitesimal time step δt, the optimal path moves with velocity $\mathbf{v}$ and continues optimally thereafter from the updated position $\mathbf{x} - \mathbf{v}\,\delta t$

$$S(\mathbf{x}) = \inf_{\mathbf{v}\in\mathbb{R}^N}\Big\{S(\mathbf{x} - \mathbf{v}\delta t) + L(\mathbf{v},\mathbf{x})\,\delta t + \mathcal{O}(\delta t^2)\Big\} \tag{11}$$

$$= \inf_{\mathbf{v}\in\mathbb{R}^N}\Big\{S(\mathbf{x}) - \mathbf{v}\cdot\nabla_{\mathbf{x}} S(\mathbf{x})\,\delta t + L(\mathbf{v},\mathbf{x})\,\delta t + \mathcal{O}(\delta t^2)\Big\}, \tag{12}$$

$$\Rightarrow \quad 0 = \inf_{\mathbf{v}\in\mathbb{R}^N}\Big\{L(\mathbf{v},\mathbf{x}) - \mathbf{v}\cdot\nabla_{\mathbf{x}} S(\mathbf{x}) + \mathcal{O}(\delta t)\Big\}. \tag{13}$$

Canceling $S(\mathbf{x})$ and retaining terms of order δt, the Hamiltonian is obtained via a Legendre transform

$$H(\mathbf{x},\mathbf{p}) := \sup_{\mathbf{v}}\Big\{\mathbf{p}\cdot\mathbf{v} - L(\mathbf{v},\mathbf{x})\Big\}, \qquad \mathbf{p} = \nabla_{\mathbf{x}} S(\mathbf{x}), \tag{14}$$

$$= \mathbf{p}\cdot\mathbf{f}(\mathbf{x}) + \|\mathbf{p}\|^2. \tag{15}$$

The minimizing action $S(\mathbf{x})$ is therefore characterized by the Hamilton–Jacobi PDE

$$H(\mathbf{x}, \nabla_{\mathbf{x}} S) = \|\nabla_{\mathbf{x}} S(\mathbf{x})\|^2 + \mathbf{f}(\mathbf{x})\cdot\nabla_{\mathbf{x}} S(\mathbf{x}) = 0. \tag{16}$$

This equation is equivalent to the leading-order stationary Fokker–Planck equation

$$\delta\,\Delta_{\mathbf{x}} P(\mathbf{x}) - \nabla_{\mathbf{x}}\cdot\big[\mathbf{f}(\mathbf{x})P(\mathbf{x})\big] = 0, \tag{17}$$

where $P(\mathbf{x})$ is the stationary density. With the ansatz $P(\mathbf{x}) = e^{-S(\mathbf{x})/\delta}$, the PDE becomes

$$\|\nabla_{\mathbf{x}} S(\mathbf{x})\|^2 + \mathbf{f}(\mathbf{x}) \cdot \nabla_{\mathbf{x}} S(\mathbf{x}) \;=\; \delta\big[\Delta_{\mathbf{x}} S(\mathbf{x}) + \nabla_{\mathbf{x}} \cdot \mathbf{f}(\mathbf{x})\big]. \tag{18}$$

In the small-noise limit $\delta \to 0^+$, solutions of (18) converge to the Hamilton–Jacobi solution (16).

We conclude that, in systems governed by an LDP, the central task is to extract the leading-order contribution to the quasi-potential S, which directly determines the exponential scaling of escape probabilities and transition rates.

D. Summary & Main Statement

We have now formalized the dynamical system of interest (1), and expressed the problem of estimating escape probabilities in terms of the quasi-potential S, as a function of the degree of non-normality κ. When $\kappa = 1$, the system is normal; in the limit $\kappa \to \infty$, the system is "highly" non-normal. The LDP framework highlights that the key objective is to determine the leading-order dependence of S on κ.

Proposition. *In the limit of a highly non-normal system, i.e. $\kappa \gg \kappa_c$ where κ_c is a critical threshold beyond which non-normal effects dominate the dynamics, the quasi-potential can be expressed as*

$$S \;=\; \left(\frac{\kappa_c}{\kappa}\right)^2 S_{\mathit{eff}} \;+\; \mathcal{O}\Big(\big(\tfrac{\kappa_c}{\kappa}\big)^3\Big)\,. \tag{19}$$

At leading order in κ/κ_c, the exponent in (8) therefore simplifies to

$$\frac{S}{\delta} \;\approx\; \frac{S_{\mathit{eff}}}{\delta_{\mathit{eff}}}, \qquad \delta_{\mathit{eff}} \sim \kappa^2 \delta, \tag{20}$$

showing that non-normality effectively renormalizes the noise scale in Kramers-type problems, producing a significant amplification of escape rates.

The derivation of this proposition is given below. This result extends the framework of [4], which established a unifying description of amplification mechanisms in non-normal *linear* systems, to the more general case of non-normal *nonlinear* systems subject to Gaussian (thermal) fluctuations.

The parameter $\kappa_c = \omega/\beta$, where $\omega := \frac{\partial^2 \phi_y}{\partial y^2}\Big|_{y=y^*}$ (28c) and $\beta := \frac{\partial^2 \psi_y}{\partial y^2}\Big|_{y=y^*}$ (28a) quantifies the balance between two competing processes: the restorative tendency of the potential well, governed by the curvature ω, and the shear imposed by the non-normal coupling, set by β. Physically, κ_c acts as a threshold separating regimes where fluctuations are either suppressed or strongly amplified. For $\kappa < \kappa_c$, restoring forces dominate and the system behaves like a conventional stable equilibrium, with noise producing only small perturbations. Once κ exceeds κ_c, however, the shear overwhelms the local curvature, so that noise is effectively multiplied and escape rates increase dramatically. In this sense, κ_c marks the critical degree of non-normality beyond which the system undergoes a qualitative change of regime, despite its eigenvalues remaining stable.

II. NON-NORMAL AMPLIFICATION OF STOCHASTIC NOISE

Amplification of stochastic noise in *linear* non-normal systems has been studied extensively in the past [3–5]. The interplay between non-normality and nonlinearity has also been noted in hydrodynamic contexts [6].

The purpose of this section is to demonstrate that, in the limit of a "highly" non-normal system, the noise variance rescaled by the factor κ^2. In particular, assuming the existence of a unique non-normal mode [3], the dynamics can be reduced to two dimensions: one associated with the non-normal mode itself, and the other with its reaction mode. In this reduced setting, the matrix potential $\mathbf{A}$ from (2) can be written as

$$\mathbf{A}(\mathbf{x}) = \mathbf{Q}\psi(\mathbf{x}), \qquad \mathbf{Q} = \begin{pmatrix} 0 & 1 \\ -1 & 0 \end{pmatrix}, \qquad \psi(\mathbf{x}) = \kappa\, \psi_y(y) - \kappa^{-1}\psi_x(x). \tag{21}$$

Note that the scalar potential $\psi(\mathbf{x})$ is separable in x and y. We also assume a separable scalar potential for ϕ, i.e. $\phi(\mathbf{x}) = \phi_x(x) + \phi_y(y)$. The generalized force (2) then takes the form

$$\mathbf{f}(\mathbf{x}) = -\nabla\phi(\mathbf{x}) + \mathbf{Q}\nabla\psi(\mathbf{x}). \tag{22}$$

Accordingly, the Jacobian of $\mathbf{f}$ at each point $\mathbf{x} = (x, y)$ is given by

$$\mathbf{J}(\mathbf{x}) := D\mathbf{f}(\mathbf{x}) = \begin{pmatrix} -\partial_x^2\phi_x(x) & \kappa\,\partial_y\psi_y(y) \\ \kappa^{-1}\partial_x^2\psi_x(x) & -\partial_y^2\phi_y(y) \end{pmatrix}. \tag{23}$$

The corresponding eigenvalues are

$$\lambda_{\pm}(\mathbf{x}) = -\tfrac{1}{2}\big(\partial_x^2\phi_x(x) + \partial_y^2\phi_y(y)\big) \;\pm\; \tfrac{1}{2}\sqrt{\big(\partial_x^2\phi_x(x) - \partial_y^2\phi_y(y)\big)^2 + 4\,\partial_y^2\psi_y(y)\,\partial_x^2\psi_x(x)}. \tag{24}$$

Remarkably, the degree of non-normality κ does not appear in the spectrum. Thus, we obtain a reduced two-dimensional nonlinear system in which the stability is governed solely by the potentials ϕ_i and ψ_i $(i = x, y)$, while non-normality manifests exclusively through a shear controlled by κ. As κ increases, the magnitude of this shear grows.

Our objective in what follows is to analyze how the quasi-potential S depends on κ, and thereby deduce the scaling of transition rates with the degree of non-normality.

A. Effective Quasi-Potential

For the system defined by (1) with the force field given by (22), the action functional (7) can be decomposed as

$$S_\tau[\mathbf{x}] = S_\tau^x[x,y] + S_\tau^y[x,y], \tag{25a}$$

$$S_\tau^x[x,y] = \frac{1}{4}\int_0^\tau \big\|\dot{x} + \partial_x\phi_x(x) - \kappa\,\partial_y\psi_y(y)\big\|^2 dt, \tag{25b}$$

$$S_\tau^y[x,y] = \frac{1}{4}\int_0^\tau \big\|\dot{y} + \partial_y\phi_y(y) - \kappa^{-1}\partial_x\psi_x(x)\big\|^2 dt. \tag{25c}$$

To minimize the action (7), the force $\mathbf{f}(\mathbf{x})$ must remain of order $\mathcal{O}(1)$ along the optimal trajectory. This requires the non-normal shear contribution $\kappa\,\partial_y\psi_y(y)$ to remain at most $\mathcal{O}(1)$.

In the limit $\kappa \to \infty$, the dynamics along the non-normal mode can be expanded near an equilibrium point y^* as

$$y = y^* + \kappa^{-1}z + \mathcal{O}(\kappa^{-2}), \qquad \text{with} \quad \partial_y\phi_y\big|_{y=y^*} = 0. \tag{26}$$

Expanding the non-normal shear term in powers of κ^{-1} yields

$$\kappa\,\partial_y\psi_y(y) = \kappa\,\partial_y\psi_y(y^*) + \partial_y^2\psi_y(y^*)\,z + \mathcal{O}(\kappa^{-1}). \tag{27}$$

Since $\kappa\,\partial_y\psi_y(y^*)$ must remain at most $\mathcal{O}(1)$, y^* must also be a zero of $\partial_y\psi_y$. Thus, the action functionals simplify to

$$S_\tau^x[x,y] = \frac{1}{4}\int_0^\tau \big\|\dot{x} + \partial_x\phi_x(x) - \beta z + \mathcal{O}(\kappa^{-1})\big\|^2 dt, \qquad \beta := \partial_y^2\psi_y\big|_{y=y^*}, \tag{28a}$$

$$S_\tau^y[x,y] = \kappa^{-2}S_\tau^z[x,z], \tag{28b}$$

$$S_\tau^z[x,z] = \frac{1}{4}\int_0^\tau \big\|\dot{z} + \omega z - \partial_x\psi_x(x) + \mathcal{O}(\kappa^{-1})\big\|^2 dt, \qquad \omega := \partial_y^2\phi_y\big|_{y=y^*}. \tag{28c}$$

Since $S_\tau^y[x,y] = \mathcal{O}(\kappa^{-2})$ while $S_\tau^x[x,y] = \mathcal{O}(1)$, minimizing the action with respect to z gives, up to $\mathcal{O}(1)$,

$$\dot{x} + \partial_x\phi_x(x) - \beta z + \mathcal{O}(\kappa^{-1}) = 0 \quad \Rightarrow \quad z = \frac{1}{\beta}\big[\dot{x} + \partial_x\phi_x(x)\big] + \mathcal{O}(\kappa^{-1}). \tag{29}$$

This cancels the leading-order contribution from S_τ^x, leaving the reduced problem

$$S_\tau[\mathbf{x}] = \kappa^{-2}S_\tau^z[x,z] + \mathcal{O}(\kappa^{-3}), \qquad \text{subject to } \dot{x} + \partial_x\phi_x(x) = \beta z. \tag{30}$$

Substituting this constraint into the reduced action, and using

$$\dot{z} = \tfrac{1}{\beta}\big[\ddot{x} + \partial_x^2\phi_x(x)\,\dot{x}\big], \tag{31}$$

we obtain the effective action functional

$$S_\tau^{\text{eff}}[x] = \frac{1}{4\beta^2}\int_0^\tau \big[\ddot{x} + (\partial_x^2\phi_x(x) + \omega)\dot{x} + \omega\,\partial_x\phi_x(x) - \beta\,\partial_x\psi_x(x)\big]^2 dt. \tag{32}$$

Hence, the quasi-potential takes the asymptotic form

$$S = \kappa^{-2}S_{\text{eff}} + \mathcal{O}(\kappa^{-3}). \tag{33}$$

In summary, the quasi-potential S admits an effective one-dimensional representation, where the impact of non-normality appears solely as a κ^{-2} scaling. Thus, in the highly non-normal regime, the escape problem is reduced to an effective single-mode description, with κ controlling the rescaling of the noise amplification.

B. Leading-Order Dynamics

In the previous section, we established that the leading-order behavior of the quasi-potential S scales as κ^{-2}. This follows from the observation that, at leading order, the influence of $\dot{y}$ vanishes, so that the action functional contributes only at order κ^{-2}.

Here, we derive the effective leading-order dynamics. We begin by expanding the dynamics of y around its equilibrium y^*

$$\dot{y} = -\partial_y \phi_y(y) + \kappa^{-1} \partial_x \psi_x(x) + \sqrt{2\delta}\, \eta_y. \tag{34}$$

Introducing the rescaled coordinate z as in (26), we obtain

$$\dot{z} = -\omega z + \partial_x \psi_x(x) + \kappa \sqrt{2\delta}\, \eta_y + \mathcal{O}(\kappa^{-1}), \tag{35}$$

where $\omega := \partial_y^2 \phi_y(y^*)$.

In the fast-recovery regime $\omega \gg 1$, this reduces to

$$z = \frac{1}{\omega}\, \partial_x \psi_x(x) + \frac{\kappa}{\omega} \sqrt{2\delta}\, \eta_y + \mathcal{O}(\kappa^{-1}). \tag{36}$$

Substituting into the dynamics of x yields

$$\dot{x} = -\partial_x \phi_x(x) + \frac{\beta}{\omega}\, \partial_x \psi_x(x) + \frac{\kappa\beta}{\omega} \sqrt{2\delta}\, \eta_y + \sqrt{2\delta}\, \eta_x + \mathcal{O}(\kappa^{-1}), \tag{37}$$

with $\beta := \partial_y^2 \psi_y(y^*)$.

Neglecting $\mathcal{O}(\kappa^{-1})$ terms, the effective leading-order dynamics becomes

$$\dot{x} = -\partial_x \phi_x(x) + \frac{1}{\kappa_c}\, \partial_x \psi_x(x) + \sqrt{2\delta_{\text{eff}}}\, \eta_x, \qquad \delta_{\text{eff}} = \delta\left(1 + \left(\tfrac{\kappa}{\kappa_c}\right)^2\right), \qquad \kappa_c = \frac{\omega}{\beta}. \tag{38}$$

This result is consistent with the effective action derived in (32), valid in the regime $\kappa \gg \kappa_c$ and under the assumption of fast mean reversion along the z direction, i.e. $\omega \gg |\partial_x^2 \phi_x(x)|$. In this limit, the quasi-potential takes the form

$$S[\mathbf{x}] \approx \frac{1}{4} \left(\frac{\kappa_c}{\kappa}\right)^2 \int_0^\tau \left[\dot{x} + \partial_x \phi_x(x) - \tfrac{1}{\kappa_c} \partial_x \psi_x(x)\right]^2 dt. \tag{39}$$

Thus, by invoking the fast-recovery approximation for the non-normal mode, we recover a rescaling of the noise amplitude δ by a factor of κ^2. Consequently, the quasi-potential S is rescaled by κ^{-2}, which captures the leading-order behavior in the limit $\kappa \gg \kappa_c$.

C. Hamilton–Jacobi

In the previous section, we showed that the leading-order behavior of the quasi-potential S scales as κ^{-2}, since at this order the influence of $\dot{y}$ vanishes, and the action functional contributes only at order κ^{-2}.

We now recover the same scaling using the Hamilton–Jacobi framework (16). As before, we assume that ϕ_y and ψ_y share the same equilibrium y^*, and employ the expansions in (3) and (27). Under these assumptions, the Hamilton–Jacobi equation (16) becomes

$$(\partial_y S)^2 + (\partial_x S)^2 + \left(\kappa\, \partial_y \psi_y - \partial_x \phi_x\right) \partial_x S + \left(\kappa^{-1} \partial_x \psi_x - \partial_y \phi_y\right) \partial_y S = 0, \tag{40a}$$

$$\Rightarrow \quad \kappa^2 (\partial_z S)^2 + (\partial_x S)^2 + \left(\beta z - \partial_x \phi_x(x) + \mathcal{O}(\kappa^{-1})\right) \partial_x S + \kappa^{-1} \left(\partial_x \psi_x - \omega z + \mathcal{O}(\kappa^{-1})\right)(\kappa\, \partial_z S) = 0, \qquad \text{since } \partial_y = \kappa\, \partial_z, \tag{40b}$$

with $\beta := \partial_y^2 \psi_y(y^*)$ and $\omega := \partial_y^2 \phi_y(y^*)$.

Asymptotic expansion. Note that $\kappa\, \partial_z S$ is not $\mathcal{O}(\kappa)$ but $\mathcal{O}(1)$, since if $S(x, y)$ is smooth in y and $y = y^* + \kappa^{-1} z$, then

$$S(x, y) = \sum_{n=0}^{\infty} S^{(n)}(x) \left(\frac{z}{\kappa}\right)^n, \qquad S^{(n)}(x) = \frac{1}{n!} \left.\frac{\partial^n S}{\partial y^n}\right|_{y=y^*}. \tag{41}$$

Hence

$$\kappa\,\partial_z S = \sum_{n=0}^{\infty} (n+1)\, S^{(n+1)}(x) \left(\frac{z}{\kappa}\right)^n . \tag{42}$$

Expanding the Hamilton–Jacobi equation in powers of z/κ, the $\mathcal{O}(1)$ term yields

$$\big(S^{(1)}(x)\big)^2 + \big(\partial_x S^{(0)}(x)\big)^2 + \big(\beta z - \partial_x \phi_x(x)\big)\, \partial_x S^{(0)}(x) = 0. \tag{43}$$

Since the coefficients $S^{(n)}(x)$ are independent of z, this forces $\partial_x S^{(0)}(x) = 0$, so that $S^{(0)}$ is constant, and also $S^{(1)}(x) = 0$. Thus, the leading-order structure of S is

$$S(x,y) = S^{(0)} + \kappa^{-2} S^{(2)}(x)\, z^2 + \mathcal{O}(\kappa^{-3}). \tag{44}$$

Next order. At $\mathcal{O}(\kappa^{-2})$, the Hamilton–Jacobi equation becomes

$$4z^2\big(S^{(2)}(x)\big)^2 + \big(\beta z - \partial_x \phi_x(x)\big)\, z^2\, \partial_x S^{(2)}(x) + \big(\partial_x \psi_x(x) - \omega z\big)\, z\, S^{(2)}(x) = 0. \tag{45}$$

Since $S^{(2)}(x)$ is independent of z, one would naively set $\partial_x S^{(2)}(x) = 0$, implying $S^{(2)}(x) = 0$. However, this contradicts the previous results. To resolve this, we incorporate the trajectory constraint

$$z = \frac{1}{\beta}\, \partial_x \phi_x(x). \tag{46}$$

Substituting yields

$$z\, S^{(2)}(x) = \tfrac{1}{2}\left(\tfrac{\omega}{\beta}\, \partial_x \phi_x(x) - \partial_x \psi_x(x)\right). \tag{47}$$

First-order solution. The Hamilton–Jacobi solution then reads

$$S(x,y) = S^{(0)} + \frac{1}{2}\left(\frac{\kappa_c}{\kappa}\right)^2 \frac{\partial_x \phi_x(x)}{\omega}\left[\partial_x \phi_x(x) - \frac{1}{\kappa_c}\partial_x \psi_x(x)\right], \tag{48}$$

where $\kappa_c = \omega/\beta$.

This expression is fully consistent with the previous derivations: the leading-order correction scales as $(\kappa_c/\kappa)^2$, and involves the same combination of potentials $\partial_x \phi_x(x) - \frac{1}{\kappa_c}\partial_x \psi_x(x)$ as in (32) and (39).

D. Validity of the WKB Approximation

In the previous sections, we have shown three complementary methods leading to the same conclusion: the quasi-potential S admits a leading-order term proportional to $(\kappa_c/\kappa)^2$. Equivalently, this scaling corresponds to a rescaling of the noise amplitude by a factor $(\kappa/\kappa_c)^2$ in the limit $\kappa \gg \kappa_c$. Thus, the effective noise level is given by $\delta_{\text{eff}} \sim \kappa^2 \delta$. However, this derivation relied on a WKB approximation, which assumes that the noise intensity δ is sufficiently small. To justify this approximation, we show that the amplification of δ by κ^2 occurs only at leading order, and not in the full expansion.

Two-scale expansion. From the Fokker–Planck equation (18), we expand the quasi-potential in powers of δ

$$S(x,y) = \sum_{n=0}^{\infty} \delta^n S_n(x,y). \tag{49}$$

At each order we obtain

$$\mathcal{O}(1): \quad \|\nabla_{\mathbf{x}} S_0(\mathbf{x})\|^2 + \mathbf{f}(\mathbf{x}) \cdot \nabla_{\mathbf{x}} S_0(\mathbf{x}) = 0, \tag{50a}$$

$$\mathcal{O}(\delta): \quad 2\nabla_{\mathbf{x}} S_0(\mathbf{x}) \cdot \nabla_{\mathbf{x}} S_1(\mathbf{x}) + \mathbf{f}(\mathbf{x}) \cdot \nabla_{\mathbf{x}} S_1(\mathbf{x}) = \Delta_{\mathbf{x}} S_0(\mathbf{x}) + \nabla_{\mathbf{x}} \cdot \mathbf{f}(\mathbf{x}), \tag{50b}$$

$$\mathcal{O}(\delta^n): \quad \sum_{k=0}^{n} \nabla_{\mathbf{x}} S_k(\mathbf{x}) \cdot \nabla_{\mathbf{x}} S_{n-k}(\mathbf{x}) + \mathbf{f}(\mathbf{x}) \cdot \nabla_{\mathbf{x}} S_n(\mathbf{x}) = \Delta_{\mathbf{x}} S_{n-1}(\mathbf{x}), \quad n \geq 2. \tag{50c}$$

For each coefficient $S_n(x,y)$, we introduce a second expansion in $1/\kappa$

$$S_n(x,y) = \sum_{m=0}^{\infty} \kappa^{-m} S_n^{(m)}(x,y). \tag{51}$$

Conclusion. The scaling $\delta_{\text{eff}} \sim \kappa^2\delta$ emerges only at the leading order in both in both δ and $1/\kappa$. Higher-order corrections in the two-scale expansion do not introduce additional amplifications of this type, but instead contribute subdominant terms. This shows that the apparent growth of the effective noise level with κ reflects a leading-order renormalization rather than a breakdown of the asymptotics. Consequently, the WKB approximation remains internally consistent: although δ_{eff} may become significantly larger than the bare noise δ, the expansion is still controlled by the small parameter δ, ensuring the validity of the quasi-potential analysis and of the WKB approximation in this regime.

E. Kramers Escape Rate

We now focus on the escape rate of the system. Neglecting terms of order $\mathcal{O}(\kappa^{-1})$, the two-dimensional dynamics in (x,y) reduce to an effective one-dimensional dynamics in x

$$\dot{x} = -U'_{\text{eff}}(x) + \sqrt{2\delta_{\text{eff}}}\,\eta, \tag{52a}$$

$$U'_{\text{eff}}(x) = \partial_x\phi_x(x) - \frac{1}{\kappa_c}\partial_x\psi_x(x), \qquad \delta_{\text{eff}} = \delta\left(1 + \left(\frac{\kappa}{\kappa_c}\right)^2\right). \tag{52b}$$

If x_i denotes a stable equilibrium and x_f the corresponding unstable point, the Kramers escape rate is

$$\Gamma = \frac{1}{2\pi}\sqrt{U''_{\text{eff}}(x_i)\left|U''_{\text{eff}}(x_f)\right|}\exp\left[-\frac{\Delta E_{\text{eff}}}{2\delta_{\text{eff}}}\right], \quad \text{where } \Delta E_{\text{eff}} = U_{\text{eff}}(x_f) - U_{\text{eff}}(x_i) \tag{53}$$

is the effective potential barrier height.

Discussion. This derivation is formally valid only in the small-noise regime. Here, however, the effective noise δ_{eff} is rescaled by $(\kappa/\kappa_c)^2$. Whether the Kramers formula remains valid depends on the balance between δ and κ/κ_c.

For example, suppose initially $2\delta \sim 10^{-2}\Delta E_{\text{eff}}$. In the normal case $\kappa \ll \kappa_c$, the escape rate is extremely small, $\Gamma \sim 3\times 10^{-44}$, implying that the system remains in its initial state for all practical purposes: the expected transition time is so large that one would need to wait astronomical timescales to observe a single escape. Now, if $(\kappa/\kappa_c)^2 = 50$, then $2\delta_{\text{eff}} \sim \Delta E_{\text{eff}}/2$, so that $\delta_{\text{eff}} \sim \Delta E_{\text{eff}}/4$. In this regime, the exponential suppression is much weaker, and we obtain $\Gamma \sim 0.13$.

Thus, the system transitions from near-perfect stability to escaping on timescales of order 10 in dimensionless units. Even though non-normality rescales the noise amplitude, the dynamics remain within the validity domain of the Kramers problem, while the escape rate can increase by many orders of magnitude.

F. Generalization with Momentum

So far, our discussion of non-normal amplification has focused on overdamped Langevin dynamics. To demonstrate that the effect is not restricted to this limit, we now consider the more general *underdamped* case, where inertia plays a role. Specifically, we study the coupled dynamics

$$\ddot{x} + \gamma\dot{x} = -\partial_x\phi_x(x) + \kappa\,\partial_y\psi_y(y) + \sqrt{2\delta}\,\eta_x, \tag{54a}$$

$$\ddot{y} + \gamma\dot{y} = -\partial_y\phi_y(y) + \kappa^{-1}\partial_x\psi_x(x) + \sqrt{2\delta}\,\eta_y, \tag{54b}$$

where γ is the linear friction coefficient. This system is the natural generalization of the overdamped equations (Sec. II A), now including second-order derivatives.

Action functional. Following the Onsager-Machlup formulation, the action functional is

$$S_\tau[x,y] = S^x_\tau[x,y] + S^y_\tau[x,y], \tag{55a}$$

$$S^x_\tau[x,y] = \tfrac{1}{4}\int_0^\tau \left[\ddot{x} + \gamma\dot{x} + \partial_x\phi_x(x) - \kappa\,\partial_y\psi_y(y)\right]^2 d\tau, \tag{55b}$$

$$S^y_\tau[x,y] = \tfrac{1}{4}\int_0^\tau \left[\ddot{y} + \gamma\dot{y} + \partial_y\phi_y(y) - \kappa^{-1}\partial_x\psi_x(x)\right]^2 d\tau. \tag{55c}$$

As in the overdamped case, we expand around a reference point $y = y^*$ satisfying $\partial_y \phi_y(y^*) = \partial_y \psi_y(y^*) = 0$, and parametrize $y = y^* + \kappa^{-1} z + \mathcal{O}(\kappa^{-2})$.

Expansion. To leading order in κ^{-1},

$$S_\tau^x[x,y] = \tfrac{1}{4}\int_0^\tau \left[\ddot{x} + \gamma\dot{x} + \partial_x\phi_x(x) - \beta z\right]^2 d\tau + \mathcal{O}(\kappa^{-1}), \qquad \beta := \partial_y^2 \psi_y(y^*), \tag{56a}$$

$$S_\tau^y[x,y] = \tfrac{1}{4\kappa^2}\int_0^\tau \left[\ddot{z} + \gamma\dot{z} + \omega z - \partial_x\psi_x(x)\right]^2 d\tau + \mathcal{O}(\kappa^{-3}), \qquad \omega := \partial_y^2 \phi_y(y^*). \tag{56b}$$

Eliminating z at leading order gives

$$z = \frac{1}{\beta}\left[\ddot{x} + \gamma\dot{x} + \partial_x\phi_x(x)\right], \tag{57}$$

so that

$$S_\tau[x,y] = \frac{1}{\kappa^2} S_\tau[x,z] + \mathcal{O}(\kappa^{-3}), \tag{58a}$$

$$S_\tau[x,z] = \tfrac{1}{4}\int_0^\tau \left[\ddot{z} + \gamma\dot{z} + \omega z - \partial_x\psi_x(x)\right]^2 d\tau. \tag{58b}$$

Inserting the constraint for z yields a fourth-order functional in x, consistent with the fact that boundary data must be specified for both positions and velocities $(x, \dot{x}, y, \dot{y})$.

Fast mean-reversion limit. Under the assumption of fast relaxation in y (i.e. $\omega \gg 1$), and defining the critical ratio $\kappa_c := \omega/\beta$, the action reduces to

$$S_\tau[x,y] \approx \frac{1}{4}\left(\frac{\kappa_c}{\kappa}\right)^2 \int_0^\tau \left[\ddot{x} + \gamma\dot{x} + \partial_x\phi_x(x) - \tfrac{1}{\kappa_c}\partial_x\psi_x(x)\right]^2 d\tau. \tag{59}$$

This is precisely the underdamped Kramers action, but with a renormalized noise amplitude rescaled by $(\kappa/\kappa_c)^2$ and a modified potential term.

Equivalent Langevin dynamics. In the same limit, y relaxes to

$$y \approx \frac{1}{\beta}\left[\kappa^{-1}\partial_x\psi_x(x) + \sqrt{2\delta}\,\eta_y\right]. \tag{60}$$

Substituting into (54) gives

$$\ddot{x} + \gamma\dot{x} \approx -\partial_x\phi_x(x) + \frac{1}{\kappa_c}\partial_x\psi_x(x) + \sqrt{2\delta\left(1 + (\tfrac{\kappa}{\kappa_c})^2\right)}\,\eta, \tag{61}$$

which reproduces the effective action (59).

Conclusion. Thus, even in the presence of inertia, non-normal coupling rescales the effective noise amplitude in exactly the same way as in the overdamped limit (Sec. II A). The amplification mechanism is therefore a general feature of non-normal stochastic systems, independent of whether momentum is included.

G. Conclusion

In this section, we have analyzed how non-normality amplifies stochastic noise and reshapes the escape dynamics of nonlinear systems. Starting from the action functional and its Hamilton–Jacobi formulation, we demonstrated that, in the highly non-normal regime $\kappa \gg \kappa_c$, the quasi-potential S is rescaled by a factor κ^{-2}. Equivalently, the system experiences an effective noise level $\delta_{\text{eff}} \sim \kappa^2\delta$, so that non-normality acts as a multiplicative noise-amplification mechanism.

We confirmed this result using three complementary approaches: (i) direct minimization of the action functional, (ii) analysis of the leading-order dynamics under a fast-recovery approximation, and (iii) expansion of the Hamilton–Jacobi equation. All methods consistently yield the same scaling law, validating both the internal consistency of the analysis and the robustness of the conclusion. Furthermore, by performing a double expansion in δ and $1/\kappa$, we justified the use of the WKB approximation and clarified that the rescaling applies only at leading order, ensuring asymptotic validity.

Finally, we applied these results to the Kramers escape problem, showing that the escape rate can increase by many orders of magnitude when κ grows, while still remaining within the validity domain of the small-noise approximation. This implies that non-normality not only destabilizes equilibria through deterministic shear, but also drastically enhances stochastic transitions by renormalizing the effective noise scale. As a consequence, systems that would otherwise appear nearly stable may exhibit frequent noise-induced escapes once non-normal amplification is taken into account.

In summary, non-normality provides a universal and quantitatively precise mechanism for stochastic amplification: it rescales the quasi-potential barrier by $(\kappa_c/\kappa)^2$ and the noise intensity by κ^2, leading to exponentially enhanced transition rates in the highly non-normal regime.

III. NUMERICAL APPLICATION

To test the validity of our theoretical derivations, we now turn to numerical experiments. We construct a minimal nonlinear model with two potential wells along the reaction (x), for which we can explicitly control the degree of non-normality κ and compare simulations with theoretical predictions.

A. Symmetric Potential Well

The minimal scalar potential with two stable equilibria and one unstable equilibrium is defined by

$$\phi(x) = \frac{\omega}{8}x^2(x^2 - 2), \quad \omega > 0, \tag{62}$$

where ω controls the mean-reversion rate at the stable points. This potential has symmetric wells with stable equilibria at $x = \pm 1$ and an unstable point at $x = 0$.

For simplicity, we take

$$\phi_x(x) = \phi(x), \qquad \phi_y(y) = \phi(y), \tag{63}$$

so that, in the absence of a solenoidal component, the system admits four stable equilibria $(\pm 1, \pm 1)$ and two unstable axes along $x = 0$ and $y = 0$.

To introduce a solenoidal contribution that preserves the equilibrium structure, we define

$$\psi(x) = \frac{\beta}{6}x(3 - x^2), \tag{64}$$

for which $\partial_x\psi(x = \pm 1) = 0$. Hence, the solenoidal component does not alter equilibrium stability. We then set $\psi_x(x) = \psi(x)$ and $\psi_y(y) = \psi(y)$.

The full system reads

$$\dot{x} = -\partial_x\phi(x) + \kappa\partial_y\psi(y) + \sqrt{2\delta}\,\eta_x, \tag{65a}$$

$$\dot{y} = -\partial_y\phi(y) + \kappa^{-1}\partial_x\psi(x) + \sqrt{2\delta}\,\eta_y, \tag{65b}$$

where η_x, η_y are independent unit white noises.

One can also note that, in the neighborhood of any stable equilibrium, the Jacobian of the generalized force field takes the form

$$\mathbf{J} = \begin{pmatrix} -\omega & \pm\beta \\ \pm\beta & -\omega \end{pmatrix}, \tag{66}$$

where the sign $\pm$ depends on which equilibrium $(x, y) = (\pm 1, \pm 1)$ the system is linearized around. The corresponding eigenvalues can be written, without loss of generality, as

$$\lambda_\pm = -\omega \pm \beta\chi, \tag{67}$$

with $\chi = 1$ for the equilibria on the diagonal ($x = y = \pm 1$) and $\chi = i$ for the off-diagonal equilibria ($x = -y = \pm 1$).

Recall that we defined the critical degree of non-normality as $\kappa_c = \omega/\beta$. This recovers the same notion of criticality introduced in [4]: pseudo-critical amplification occurs when $\kappa > \kappa_c$, with κ_c scaling proportionally to the distance from criticality (ω) and inversely to the degree of degeneracy (β). Thus, the framework of unified amplification in linear systems naturally extends to the nonlinear setting considered here.

Finally, to ensure the stability of the diagonal equilibria ($x = y = \pm 1$), the parameters must satisfy $\omega > |\beta| \geq 0$.

In the regime where $y \approx \pm 1$ is "almost stable," the effective dynamics of x reduces to

$$\dot{x} = -U'_{\text{eff}}(x) + \sqrt{2\delta_{\text{eff}}}\,\eta, \tag{68}$$

with

$$U_{\text{eff}}(x) = \phi(x) \mp \frac{1}{\kappa_c}\psi(x), \qquad \delta_{\text{eff}} = \delta\left[1 + \left(\frac{\kappa}{\kappa_c}\right)^2\right], \qquad \kappa_c = \frac{\omega}{\beta}. \tag{69}$$

The sign in $U_{\text{eff}}(x)$ depends on the choice $y^* = \pm 1$.

For an escape from $x_i = \pm 1$ to $x_f = 0$, the effective barrier and prefactor are

$$\Delta E_{\text{eff}} = \omega\left[\frac{1}{8} \mp \frac{1}{2\kappa_c^2}\right], \qquad C = \frac{1}{2\pi}\sqrt{\frac{\omega}{2}\left(1 \mp \frac{1}{\kappa_c^2}\right)}. \tag{70}$$

Thus, the dynamics is controlled by four parameters:

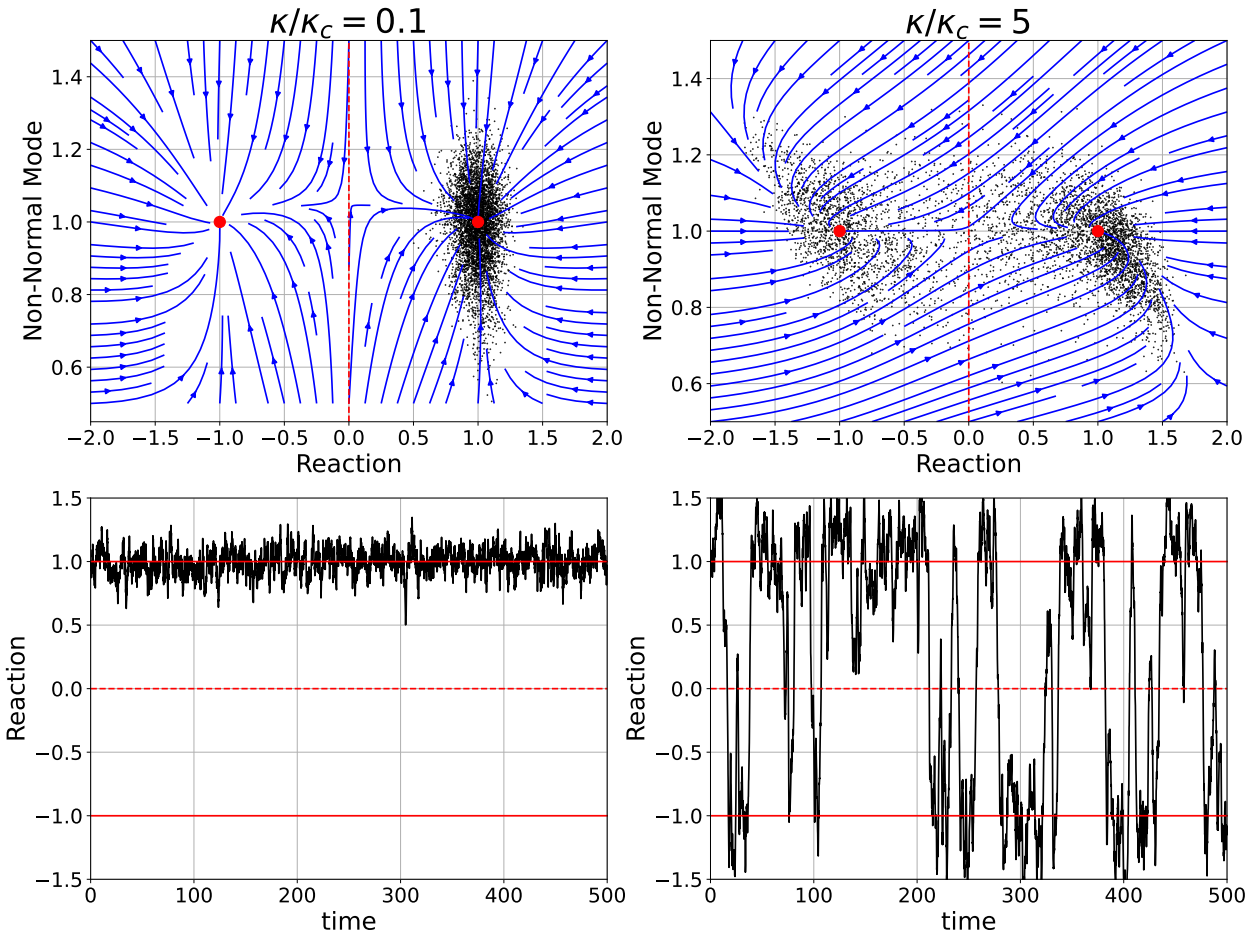

FIG. 1. Simulation of a nonlinear two-dimensional system described in Section III A, with parameters $\omega = 1$, $\delta = 0.01$, and $\kappa_c = 10$. The left panels correspond to $\kappa = \kappa_c/10$, while the right panels correspond to $\kappa = 5\kappa_c$.
Top panels: dynamics in phase space, where the horizontal axis denotes the reaction coordinate (x) and the vertical axis the non-normal mode (y). Red dots mark the stable equilibria $(x, y) = (\pm 1, 1)$, blue arrows indicate the force vector field, and the dashed red line at $x = 0$ denotes the unstable manifold along the reaction direction.
Bottom panels: time series of the reaction variable (x). Continuous red lines mark the stable equilibria at $x = \pm 1$, and the dashed red line marks the unstable equilibrium at $x = 0$.
All simulations are performed over a time horizon $T = 500$ with integration step $\Delta t = 0.1$, corresponding to $N = 5000$ time steps.

- ω : mean-reversion rate around equilibria.
- δ : amplitude of the input noise.
- κ_c : critical threshold for the restoring amplitude to non-normal shear.
- κ : actual strength of the non-normal shear.

B. Numerical Result

Figure 1 shows trajectories for $\delta = 10^{-2}$, $\omega = 1$, $\kappa_c = 10$, with $\kappa = \kappa_c$ (left) and $\kappa = 5\kappa_c$ (right). The top row displays the phase space trajectories, while the bottom row shows the dynamics of x. For $\kappa = \kappa_c$, the system remains trapped in a single well for the entire simulation, whereas for $\kappa = 5\kappa_c$, it transitions ~ 20 times between $x = \pm 1$ over the duration $T = 500$ of the simulations.

A systematic scan over κ, shown in Figure 2, confirms this transition. For $\kappa < \kappa_c$, escapes are very rare as the transition rate is exceedingly small, and the variance of x remains close to the Ornstein-Uhlenbeck prediction $\sqrt{\delta/\omega} = 1/10$. At $\kappa = \kappa_c$, a qualitative shift occurs: the system begins to transition between wells while the input noise level remains constant at a very small level, and the variance abruptly increases to ~ 1. For $\kappa > \kappa_c$, the measured escape rate converges to the theoretical prediction (70), validating both the rescaling $\delta_{\text{eff}} \sim \kappa^2\delta$ and the overall large-deviation framework.

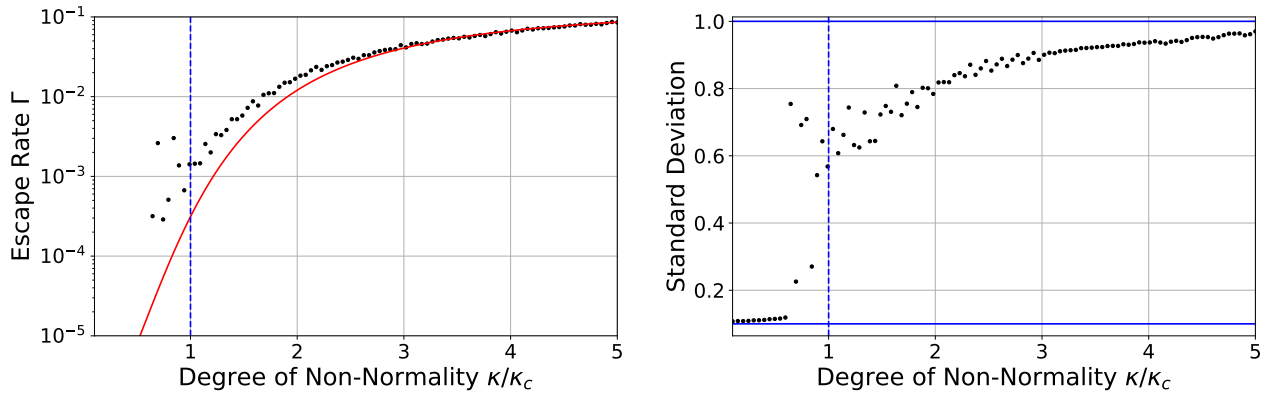

FIG. 2. Escape rate (left panel) and standard deviation (right panel) of the reaction variable (x) for the dynamics described in Section III A, with parameters $\omega = 1$, $\delta = 0.01$, and $\kappa_c = 10$, as a function of κ. Simulations are performed for κ ranging from $\kappa_c/10$ to $5\kappa_c$.
Each simulation runs over a total time $T = 10^5$ with integration step $\Delta t = 0.1$, corresponding to $N = 10^6$ data points. The escape rate is estimated as $\Gamma = 1/\langle\tau\rangle$, where $\langle\tau\rangle$ is the mean first-passage time from $x > 0$ to $x < 0$ (or vice versa). Black dots denote numerical measurements, and the red curve shows the theoretical escape rate given by Eq. (53). The vertical dashed blue line marks the critical value $\kappa = \kappa_c$. In the right panel, the lower horizontal blue line indicates the theoretical standard deviation of an Ornstein-Uhlenbeck approximation near equilibrium, $\sqrt{\delta/\omega} = 0.1$, while the upper blue line ($= 1$) corresponds to the variance of a process equally likely to be near $x = \pm 1$.

C. Asymmetric Potential Well

In the previous section, we studied the symmetric case, where the dynamics of the reaction variable x is nearly symmetric, so that the transition rates between the two stable equilibria are identical. We now introduce an asymmetry by modifying the scalar and solenoidal potentials along x, defined as

$$\phi_x(x) = \frac{\omega}{1+\Delta}\frac{1}{4}x^2\left[x^2 + \frac{4}{3}(\Delta-1)x - 2\Delta\right], \qquad \psi_x(x) = \frac{\beta}{1+\Delta}\frac{1}{3}x\left[x^2 + \frac{3}{2}(\Delta-1)x - 3\Delta\right], \tag{71}$$

whose derivatives are

$$\partial_x\phi_x(x) = \frac{\omega}{1+\Delta}x(x-1)(x+\Delta), \qquad \partial_x\psi_x(x) = \frac{\beta}{1+\Delta}(x-1)(x+\Delta). \tag{72}$$

For $\Delta > 1$, the system retains one unstable equilibrium at $x = 0$, but the two stable equilibria are now located at $x = 1$ and $x = -\Delta$. Crucially, the heights of the potential barriers separating these equilibria are no longer identical.

Keeping the potentials along the y-direction unchanged from Section III A, the critical degree of non-normality remains $\kappa_c = \omega/\beta$. The effective potential barrier from $x = 1$ to $x = 0$ is then

$$\Delta E_{\text{eff},1} = \frac{\omega}{1+\Delta}\left[\frac{1}{12}(1+2\Delta) - \frac{1}{6\kappa_c^2}(1+3\Delta)\right]. \tag{73}$$

For $\Delta = 1$, this reduces to the symmetric case of Eq. (70), while in the limit $\Delta \to \infty$, the barrier remains of order $\mathcal{O}(1)$.

In contrast, the effective barrier from $x = -\Delta$ to $x = 0$ is

$$\Delta E_{\text{eff},-\Delta} = \frac{\omega\Delta^2}{1+\Delta}\left[\frac{1}{12}(\Delta+2) + \frac{1}{6\kappa_c^2}(\Delta+3)\right], \tag{74}$$

which grows as $\mathcal{O}(\Delta^2)$ in the limit $\Delta \to \infty$.

Thus, the asymmetric potential well provides a bistable system in which non-normality can induce sufficiently large fluctuations to overcome the barrier in one direction, while the reverse transition remains exponentially suppressed. This construction highlights how non-normal amplification can break reversibility in noise-induced transitions.

D. Conclusion

Through the numerical study of symmetric and asymmetric bistable potentials, we have validated the theoretical prediction that the quasi-potential is rescaled by a factor $(\kappa_c/\kappa)^2$, where the critical degree of non-normality

$\kappa_c = \omega/\beta$ acts as the threshold separating regimes where non-normal amplification is negligible ($\kappa < \kappa_c$) or dominant ($\kappa > \kappa_c$). This provides a clear interpretation of κ_c: it links the strength of non-normal shear to the intrinsic stability of the system, so that criticality in the reversible (gradient) part of the dynamics and the non-normal amplification mechanism are tied together.

Studying bistable potentials is particularly insightful, since transitions between stable equilibria are the most direct manifestation of stochastic fluctuations. In the symmetric case, we observed that the onset of non-normality induces a sudden increase in transition rates, while in the asymmetric case, the same mechanism selectively amplifies fluctuations in one direction, leading to irreversible dynamics where escape is favored only from one potential well. This demonstrates that non-normal amplification not only accelerates noise-induced transitions, but can also fundamentally alter the symmetry and reversibility of the system's long-term behavior.

Finally, although we restricted the analysis to quartic potentials generating bistability, the framework is not limited to this case. Higher-order polynomials can be used to construct systems with multiple stable equilibria, thus extending the analysis to multistable landscapes. In all cases, however, the transitions along the reaction coordinate are expected to obey the same rule: their rates are governed by the balance between the potential restoring force and the shear strength (measured respectively by ω and β) combined in the critical degree of non-normality $\kappa_c = \omega/\beta$ and non-normal shear (measured by κ). This shows that κ/κ_c provides a universal coefficient controlling the strength and impact of non-normal amplification across a broad class of nonlinear stochastic systems.

IV. APPLICATION TO DNA METHYLATION

DNA methylation is a key epigenetic mechanism that modulates gene regulation and cellular identity. Yet methylation patterns can switch states on unexpectedly fast timescales – sometimes within minutes in response to environmental cues – challenging predictions from classical variational Kramers-type models [7]. Several biological features plausibly contribute to this rapidity: (i) chromatin architecture locally boosts DNMT access and activity, creating methylation hotspots [8], (ii) stochastic metabolic fluctuations (e.g., transient surges in S-adenosylmethionine) amplify reaction propensities [7], and (iii) positive feedback, whereby methylation at one CpG promotes methylation in neighboring regions, supports rapid propagation of marks (chemical modifications on DNA or histones that modulate gene expression without changing sequence) [9, 10]. External signals (oxidative stress, pathway activation) further reshape the methylation landscape dynamically.

Viewed through the lens of *non-normal* stochastic dynamics, these observations admit a parsimonious explanation. In non-normal systems, the solenoidal/rotational component of the force field transiently amplifies perturbations, which *renormalizes the effective noise level* and, in turn, the escape kinetics. Concretely, in the small-noise limit used throughout this SM, the dynamics along the reaction coordinate obeys an effective 1D Langevin equation, so that the Kramers rate inherits the standard form with δ replaced by δ_{eff} i.e. see (52b) and (53). This renormalization explains how methylation transitions can occur on minute timescales despite modest thermal noise: transient amplification effectively raises the temperature experienced along the escape path, while preserving the system's bistability structure.

Empirical features of DNA methylation are consistent with the three hallmarks of non-normality:

1. **Asymmetry.** DNMTs preferentially target specific sequence and chromatin contexts, biasing local dynamics.

2. **Hierarchy.** Local positive feedback enables cascading spread from hemimethylated to fully methylated regions.

3. **Stochastic fluctuations.** Variability in methyl-donor availability and enzymatic activity injects extrinsic and intrinsic noise.

Together, these place methylation dynamics squarely within the class of non-variational, highly non-normal systems. In what follows, we make this connection explicit by embedding an established bistable model of CpG dyads within our framework, adding Langevin noise, and quantifying how non-normal amplification (κ/κ_c) accelerates transitions while maintaining bistability.

A. Model

To make the connection with DNA methylation explicit, we start from the nonlinear model in [11]. This framework was developed to describe the coexistence of unmethylated, hemimethylated, and methylated CpG dyads, thereby rationalizing the experimentally observed bistability of methylation. This model captures how localized interactions and cooperative enzymatic processes drive transitions between hypo- and hypermethylated states. In its original form, the dynamics are deterministic, and noise is absent; however, the authors noted the importance of incorporating stochasticity to reflect uncertainty in methylation levels. Here, by uncertainty we mean fluctuations around the attractors corresponding to unmethylated, hemimethylated, and fully methylated

CpG dyads. We extend their formulation by explicitly embedding stochastic fluctuations within an overdamped Langevin framework, which allows us to characterize not only the variance of methylation levels but also the noise-driven transition rates between epigenetic states.

Stochastic embedding. The model in [11] can be naturally embedded into our non-normal stochastic framework. Introducing Gaussian noise terms, we obtain the coupled equations

$$\begin{cases} \dot{x}_1 = -a_{13}x_1^3 + a_{12}Cx_1^2 - a_{11}x_1 + a_{10}C - b_{13}x_1^2x_3 - b_{11}x_3 + \sqrt{2\delta}\,\eta_1, \\ \dot{x}_3 = -a_{33}x_3^3 + a_{32}Cx_3^2 - a_{31}x_3 + a_{30}C - b_{33}x_3^2x_1 - b_{31}x_1 + \sqrt{2\delta}\,\eta_3, \end{cases} \quad \text{with} \quad \eta_1, \eta_3 \overset{iid}{\sim} \mathcal{N}(0,1), \tag{75}$$

where x_1 and x_3 denote the numbers of unmethylated and methylated dyads, respectively, and the hemimethylated count is $x_2 = C - x_1 - x_3$, with $C > 0$ the total number of CpG dyads.

Hyper-parameters. The coefficients a_{ij} and b_{ij} are defined in terms of transition rates k_{ij} as

$$a_{13} = k_{32} - k_{12}, \quad a_{12} = k_{32}, \quad a_{11} = k_{11} + k_{31} + \tfrac{1}{2}D, \quad a_{10} = k_{31} + \tfrac{1}{2}D, \quad b_{13} = k_{32}, \quad b_{11} = k_{31} + \tfrac{1}{2}D, \tag{76a}$$

$$a_{33} = k_{22} - k_{42}, \quad a_{32} = k_{22}, \quad a_{31} = k_{21} + k_{41} + D, \quad a_{30} = k_{21}, \quad b_{33} = k_{22}, \quad b_{31} = k_{21}, \tag{76b}$$

with k_{ij} denoting reaction rates, in the notation of [11]. Biologically, k_{21} represents the effective methylation rate of hemimethylated dyads, k_{31} the active demethylation rate, and D the cell-division rate (which contributes to passive demethylation when maintenance is incomplete). The parameter values used in [11] are summarized in Table I.

k_{11}	k_{12}	k_{21}	k_{22}	k_{31}	k_{32}	k_{41}	k_{42}	C	D
2.1	2×10^{-5}	10	10^{-2}	1	10^{-2}	4	2×10^{-4}	100	1

TABLE I. Parameter values used in the model of [11].

Simplifications. Using Table I together with definitions (76), several simplifications follow

$$C \gg 1, \qquad a_{13} \approx a_{33} \approx a_{12} = a_{32} = b_{13} = b_{33}, \qquad a_{11} \approx a_{10} \approx b_{11}, \qquad a_{31} \approx a_{30} \approx b_{31}. \tag{77}$$

Since $x_1, x_3 \in (0, C)$, it is natural to rescale

$$x_1 = Cy_1, \qquad x_3 = Cy_3, \tag{78}$$

yielding

$$\begin{cases} \dot{y}_1 = -C^2y_1^2[a_{13}y_1 + b_{13}y_3 - a_{12}] - a_{11}y_1 + a_{10} - b_{11}y_3 + C^{-1}\sqrt{2\delta}\,\eta_1, \\ \dot{y}_3 = -C^2y_3^2[a_{33}y_3 + b_{33}y_1 - a_{32}] - a_{31}y_3 + a_{30} - b_{31}y_1 + C^{-1}\sqrt{2\delta}\,\eta_3. \end{cases} \tag{79}$$

From the parameter hierarchy, note that $a_{13}, a_{33} \sim C^{-1}$, and k_{12}, k_{32} and k_{42} are orders of magnitude lower than the other parameters. This leads to the reduced form

$$\begin{cases} \dot{y}_1 = -\big[Cy_1^2 + \omega_1\big]\big(y_1 + y_3 - 1\big) - ky_1 + C^{-1}\sqrt{2\delta}\,\eta_1, \\ \dot{y}_3 = -\big[Cy_3^2 + \omega_3\big]\big(y_1 + y_3 - 1\big) - ky_3 + C^{-1}\sqrt{2\delta}\,\eta_3, \end{cases} \tag{80}$$

where

$$\omega_i := a_{i0} = b_{i1}, \qquad k \approx k_{11}, k_{41}. \tag{81}$$

Here, we consolidate k_{11} and k_{41} into a single effective parameter k, reducing the dimensionality of the hyper-parameter set.

Time rescaling. Introducing a rescaling $t \mapsto Ct$ simplifies the system to

$$\begin{cases} \dot{y}_1 = -y_1^2\big(y_1 + y_3 - 1\big) - C^{-1}\big[\omega_1\big(y_1 + y_3 - 1\big) + ky_1\big] + C^{-3/2}\sqrt{2\delta}\,\eta_1, \\ \dot{y}_3 = -y_3^2\big(y_1 + y_3 - 1\big) - C^{-1}\big[\omega_3\big(y_1 + y_3 - 1\big) + ky_3\big] + C^{-3/2}\sqrt{2\delta}\,\eta_3. \end{cases} \tag{82}$$

Summary. Equation (82) is the reduced stochastic model that we analyze throughout this section. In the next steps, we (i) identify stable and unstable equilibria, (ii) characterize the non-normal mode and its reaction variable, and (iii) quantify the strength of the non-normal shear that determines when non-normal amplification of transition rates occurs.

B. Equilibrium Points

Our next step is to approximate the stable equilibria of the reduced model (82). Identifying these equilibria is crucial for two reasons: (i) the line connecting the two stable fixed points defines the reaction coordinate, and (ii) the non-normal mode must be orthogonal to this line. This construction provides a geometric way to separate the reaction direction from the non-normal shear.

Location of equilibria. From [11], the system admits two stable fixed points: one with $x_1 \sim C$, $x_3 \sim 1$, and the other with $x_1 \sim 1$, $x_3 \sim C$. In the rescaled variables $y_i = x_i/C$, and in the large-C limit, these equilibria correspond to $(y_1, y_3) \approx (1, C^{-1})$ and $(y_1, y_3) \approx (C^{-1}, 1)$. Both are close to the line $y_1 + y_3 = 1$. We therefore introduce rotated coordinates (z_1, z_3) defined by

$$\begin{cases} z_1 = \frac{1}{\sqrt{2}}\,(y_1 + y_3 - 1), \\ z_3 = \frac{1}{\sqrt{2}}\,(y_1 - y_3), \end{cases} \quad \Longleftrightarrow \quad \begin{cases} y_1 = \frac{1}{\sqrt{2}}\,(z_1 + z_3) + \frac{1}{2}, \\ y_3 = \frac{1}{\sqrt{2}}\,(z_1 - z_3) + \frac{1}{2}. \end{cases} \tag{83}$$

This transformation consists of a translation plus a rotation, so it preserves the system's non-normality.

Dynamics in the rotated basis. In the (z_1, z_3) variables, the deterministic part of the dynamics becomes

$$\begin{cases} \dot{z}_1 = -\left[\left(z_1 + \frac{1}{\sqrt{2}}\right)^2 + z_3^2\right] z_1 - C^{-1}(\omega_+ + k) z_1 - C^{-1}\frac{k}{\sqrt{2}}, \\ \dot{z}_3 = -2\left(z_1 + \frac{1}{\sqrt{2}}\right) z_3 z_1 - C^{-1}\big(\omega_- z_1 + k z_3\big), \end{cases} \qquad \omega_\pm = \omega_1 \pm \omega_3. \tag{84}$$

Asymptotic expansion. Because equilibria satisfy $\dot{z}_1 = \dot{z}_3 = 0$, we expand

$$z_1 = z_1^{(1)} C^{-1} + z_1^{(2)} C^{-2} + \mathcal{O}(C^{-3}), \qquad z_3 = z_3^{(0)} + z_3^{(1)} C^{-1} + \mathcal{O}(C^{-2}). \tag{85}$$

Substituting into (84) and matching powers of C^{-1} gives recursive equations for $z_1^{(j)}$ and $z_3^{(j)}$.

Order $\mathcal{O}(C^{-1})$. At leading order,

$$\begin{cases} (\frac{1}{2} + (z_3^{(0)})^2)\, z_1^{(1)} + \frac{k}{\sqrt{2}} = 0, \\ (\sqrt{2} z_1^{(1)} + k)\, z_3^{(0)} = 0, \end{cases} \quad \Longrightarrow \quad \begin{cases} z_1^{(1)} = -\sqrt{2}k, \\ z_3^{(0)} = 0, \end{cases} \quad \text{or} \quad \begin{cases} z_1^{(1)} = -\frac{k}{\sqrt{2}}, \\ z_3^{(0)} = \pm\frac{1}{\sqrt{2}}. \end{cases} \tag{86}$$

Order $\mathcal{O}(C^{-2})$. Proceeding to next order yields

$$\begin{cases} \left(\frac{1}{2} + (z_3^{(0)})^2\right) z_1^{(2)} + 2 z_3^{(0)} z_1^{(1)} z_3^{(1)} = -z_1^{(1)}\left(\sqrt{2} z_1^{(1)} + \omega_+ + k\right), \\ \sqrt{2} z_3^{(0)} z_1^{(2)} + (\sqrt{2} z_1^{(1)} + k) z_3^{(1)} = -z_1^{(1)}(2 z_1^{(1)} z_3^{(0)} + \omega_-). \end{cases} \tag{87}$$

From this, the equilibria are

$$\begin{cases} z_1^{(0)} = -\sqrt{2} k C^{-1} + \mathcal{O}(C^{-2}), \\ z_3^{(0)} = -\sqrt{2}\omega_- C^{-1} + \mathcal{O}(C^{-2}), \end{cases} \quad \text{or} \quad \begin{cases} z_1^{(\pm)} = -\frac{k}{\sqrt{2}} C^{-1} + \mathcal{O}(C^{-2}), \\ z_3^{(\pm)} = \pm\frac{1}{\sqrt{2}} - \frac{1}{\sqrt{2}} C^{-1}(\pm k \pm \omega_+ - \omega_-) + \mathcal{O}(C^{-2}). \end{cases} \tag{88}$$

Jacobian analysis. Linearizing (84) about each equilibrium yields Jacobians

$$\mathbf{J}_0 = -\begin{pmatrix} 1/2 & 0 \\ 0 & 0 \end{pmatrix} + C^{-1}\begin{pmatrix} 3k - \omega_+ & 0 \\ \omega_- & k \end{pmatrix} + \mathcal{O}(C^{-2}), \tag{89a}$$

$$\mathbf{J}_\pm = -\begin{pmatrix} 1 & 0 \\ \pm 1 & 0 \end{pmatrix} + C^{-1}\begin{pmatrix} 2k \pm \omega_- & \pm(-k) \\ \pm(3k + \omega_+) - \omega_- & 0 \end{pmatrix} + \mathcal{O}(C^{-2}), \tag{89b}$$

where $\mathbf{J}_0$ and $\mathbf{J}_\pm$ are respectively the Jacobian estimated at $\mathbf{z}_0 = (z_{1,0}\,,\, z_{3,0})$, and $\mathbf{z}_\pm = (z_{1,\pm}\,,\, z_{3,\pm})$.

Their eigenvalues are

$$\begin{cases} \lambda_{+,0} = -\frac{1}{2} + C^{-1}(3k - \omega_+) + \mathcal{O}(C^{-2}), \\ \lambda_{-,0} = C^{-1} k + \mathcal{O}(C^{-2}), \end{cases} \qquad \begin{cases} \lambda_{+,\pm} = -1 - C^{-1}(-3k \pm \omega_-) + \mathcal{O}(C^{-2}), \\ \lambda_{-,\pm} = -2kC^{-1} + \mathcal{O}(C^{-2}). \end{cases} \tag{90}$$

Conclusion. The point $\mathbf{z}_0$ is unstable, while $\mathbf{z}_\pm$ are stable equilibria. We interpret $\mathbf{z}_+$ as the methylated state and $\mathbf{z}_-$ as the unmethylated state. To obtain transition between the two states $\mathbf{z}_\pm$, we need to estimate if the system is non-normal, and it is required to have the reaction aligned along the z_3-axis.

C. Non-Normality of the System

To quantify the non-normality of the reduced dynamics (82), we compute the eigenvectors of the Jacobian at each equilibrium point $\mathbf{z}_0$ (unstable) and $\mathbf{z}_\pm$ (stable). Expanding to order $\mathcal{O}(C^{-1})$ yields

$$\mathbf{p}_{+,\pm} = \tfrac{1}{\sqrt{2}} \begin{pmatrix} 1 \\ \pm 1 \end{pmatrix} + \frac{1}{\sqrt{2}} C^{-1} \begin{pmatrix} -3k \pm \left(\omega_- - \frac{\omega_+}{2}\right) \\ \pm\left(3k + \omega_+\right) - \omega_- - \frac{\omega_+}{2} \end{pmatrix} + \mathcal{O}(C^{-2}), \quad \mathbf{p}_{-,\pm} = \begin{pmatrix} 0 \\ 1 \end{pmatrix} \pm 2C^{-1} k \begin{pmatrix} 1 \\ 0 \end{pmatrix} + \mathcal{O}(C^{-2}), \tag{91a}$$

$$\mathbf{p}_{+,0} = \begin{pmatrix} 1 \\ 0 \end{pmatrix} - 2C^{-1}\omega_- \begin{pmatrix} 0 \\ 1 \end{pmatrix} + \mathcal{O}(C^{-2}), \qquad \mathbf{p}_{-,0} = \begin{pmatrix} 0 \\ 1 \end{pmatrix} + 2C^{-1} k \begin{pmatrix} 1 \\ 0 \end{pmatrix} + \mathcal{O}(C^{-2}). \tag{91b}$$

Condition number and non-normal index. The degree of non-normality is captured by the condition number of the eigenbasis [3],

$$\kappa_i = \sqrt{\frac{1 + |\mathbf{p}_{+,i} \cdot \mathbf{p}_{-,i}|}{1 - |\mathbf{p}_{+,i} \cdot \mathbf{p}_{-,i}|}}, \tag{92}$$

where $i \in \{0, \pm\}$ denotes the equilibrium point [4]. We obtain

$$\kappa_0 = 1 + 2C^{-1}\left|k - \omega_+\right| + \mathcal{O}(C^{-2}), \qquad \kappa_\pm = \left(\sqrt{2}+1\right)\left[1 - \sqrt{2}C^{-1}\left(\pm\left(5k + \omega_+\right) - \omega_- - \frac{\omega_+}{2}\right)\right] + \mathcal{O}(C^{-2}), \tag{93}$$

therefore, close to the stable equilibrium, the system is always non-normal, but near the unstable equilibrium the system is almost normal. In all cases $\kappa_i > 1$, confirming that the system is non-normal near each equilibrium.

A convenient scalar measure is the *non-normal index* [4]

$$K_i = \tfrac{1}{2}\left(\kappa_i - \kappa_i^{-1}\right). \tag{94}$$

Comparing K_i with its critical threshold

$$K_{c,i} := \sqrt{\frac{\sqrt{\alpha_i^2 - 1}}{\alpha_i - \sqrt{\alpha_i^2 - 1}}}, \qquad \alpha_i = \left|\tfrac{\lambda_{+,i} + \lambda_{-,i}}{\lambda_{+,i} - \lambda_{-,i}}\right|, \tag{95}$$

identifies whether the system is *pseudo-critical*, meaning that transient perturbations are amplified along the reaction coordinate before decaying. For the stable equilibria, we obtain

$$K_{c,\pm} = 2^{3/4}\left(\tfrac{k}{C}\right)^{1/4} + \mathcal{O}(C^{-3/4}), \tag{96}$$

so that $K_\pm / K_{c,\pm} = \mathcal{O}(C^{1/4})$. Thus, the non-normal amplification grows with system size C. The unstable equilibrium $\mathbf{z}_0$ is naturally unstable, so perturbations there grow exponentially regardless of non-normality.

Conclusion. The DNA methylation model is strongly non-normal near its equilibria. This ensures transient deviations in the linearized dynamics, raising the key question: do these deviations enhance the transition rates between the unmethylated and methylated states?

D. Reaction and Non-Normal Mode

The stable equilibria lie near $z_1 \approx 0$, $z_3 \approx \pm 1$, but to identify how transitions occur we must separate the *reaction direction* from the *non-normal mode* that drives transient deviations [3].

SVD approach. Let $\mathbf{P}_\pm = (\mathbf{p}_{+,\pm}, \mathbf{p}_{-,\pm})$ be the eigenbasis matrix. Its singular value decomposition reads $\mathbf{P}_\pm = \mathbf{U}_\pm \mathbf{\Sigma}_\pm \mathbf{V}_\pm^\dagger$, where $\mathbf{U}_\pm$ and $\mathbf{V}_\pm$ are unitary matrices, and $\mathbf{\Sigma}_\pm$ is a diagonal matrix composed of the singular value. We identify the column of $\mathbf{U}_\pm$ associated with the largest singular value as the reaction, and the column associated with the smallest singular value as the non-normal mode.

To leading order in C^{-1}, $\mathbf{P}_\pm$ is upper triangular, giving

$$\mathbf{U}_\pm = \frac{1}{\sqrt{2}} \begin{pmatrix} 1 & 1 \\ 1 & -1 \end{pmatrix}. \tag{97}$$

Hence $\hat{\mathbf{r}} = (1\,,\,1)/\sqrt{2}$, $\hat{\mathbf{n}} = (1\,,\,-1)/\sqrt{2}$.

Implications. The reaction coordinate is therefore not aligned with the geometric axis $z_1 = 0$ connecting the equilibria. Instead, we have to estimate if non-normal amplification pushes the system toward the separatrix, the curve separating the two basins of attraction.

Near the unstable equilibrium $\mathbf{z}_0$, the separatrix is tangent to the stable eigenvector $\mathbf{p}_{+,0} \approx (1\,,\,0)$, which is aligned along z_1, and the more the system gets close to the unstable equilibrium, the more the system is normal, and so non-normal amplification will not affect the stability of the system. In this limit, the z_1-axis remains stable, while the dynamics along z_3 is unstable, so that transitions between the states $z_3 \approx +1$ and $z_3 \approx -1$ occur through Brownian-like fluctuations. Thus, although the system is non-normal around stable equilibria, its linearized non-normality alone cannot guarantee accelerated switching, in this given model.

E. Bistability and Non-Normal Acceleration

The original goal in [11] was to demonstrate the bistability of DNA methylation dynamics. Their model explains the coexistence of hypo- and hypermethylated states but cannot account for experimentally observed *fast* transitions (on the order of $\sim$ 10 minutes) [7]. In the original framework, transitions occur only near criticality, when a Jacobian eigenvalue crosses zero and the potential barrier vanishes, allowing noise to induce switching.

Beyond criticality. Our analysis combines three ingredients:

1. the system is bistable, with two long-lived methylation states;
2. transitions can occur at criticality, when a barrier disappears;
3. even away from criticality, non-normality can amplify fluctuations, renormalizing the effective noise.

To reconcile bistability with observed rapid switching, we propose the following modification

$$\begin{cases} \dot{z}_1 = -\omega_1 z_1 + \kappa^{-1}\beta(z_3 - z_{3,+})(z_3 - z_{3,-}) + \sqrt{2\delta}\,\eta_1, \\ \dot{z}_3 = -\omega_3(z_3 - z_{3,0})(z_3 - z_{3,+})(z_3 - z_{3,-}) + \kappa\beta z_1 + \sqrt{2\delta}\,\eta_3, \end{cases} \tag{98}$$

with equilibria at $(0, z_{3,\pm})$ and unstable point $(0, z_{3,0})$, such that $z_{3,+} > z_{3,0} > z_{3,-}$. This construction preserves the equilibria and their stability, but alters the flow structure so as to introduce genuine non-normal amplification, in line with Ref. [11]. This formulation reproduce the coexistence of long-term memory and fast stochastic transitions observed in methylation dynamics while preserving the equilibria and their stability. The dynamical system (98) provides an illustrative case where we minimally modify an existing model to suggest how non-normal phase transitions could manifest in biology. More broadly, DNA methylation is paradigmatic because it simultaneously exhibits "classical" bistability (which secures epigenetic memory) and "fast" stochastic switching (which enables rapid adaptation). Our framework is unique in reconciling these two features. Furthermore, by linking the non-normality index κ to the biochemical balance of DNMTs versus TET enzymes, the model acquires a direct mechanistic interpretation. In this way, we hope to attract the attention of the community to fully resolve the kinetics of DNA methylation from the non-normal dynamics perspective.

Interpretation.

- Along z_1, the system is linearly stable, consistent with [11].
- Along z_3, bistability arises from the cubic nonlinearity, with two stable equilibria and one unstable saddle.
- As $\omega_i \to 0^+$ or $z_{3,\pm} \to z_{3,0}$, the system approaches criticality.
- If $\kappa \geq \kappa_c = \omega_1/\beta$, the system enters a pseudo-critical regime: non-normality renormalizes the effective noise, enabling rapid switching even far from true criticality.

Numerical Analysis. In Figure 3, we show two simulations of the ratio of methylated and unmethylated sites, i.e. the (y_1, y_2) space defined in (83), obtained by simulating (98) with $\kappa = \kappa_c/10$ and $\kappa = 2\kappa_c$. To introduce asymmetry, we choose parameters such that $|z_{3,+} - z_{3,0}| > |z_{3,-} - z_{3,0}|$. When $\kappa < \kappa_c$, the system remains stable around both equilibria. However, as κ approaches κ_c, the system exits the stable equilibrium $z_{3,-}$ and becomes trapped around the second stable equilibrium $z_{3,+}$. This occurs because the mean-reversion rate of the dynamics of z_3 near $z_{3,+}$ is stronger than near $z_{3,-}$, as the potential barrier between $z_{3,+}$ and $z_{3,0}$ is higher than the one between $z_{3,-}$ and $z_{3,0}$.

This asymmetry between the two transition rates is made explicit in Figure 4, where we plot the measured transition rates from each equilibrium as a function of κ/κ_c. For instance, when $\kappa = 4\kappa_c$, the transition rate from $z = z_{3,-}$ to $z_{3,+}$ in the considered time unit is $\Gamma_{z_{3,-}\to\mathbf{z}_{3,-}} \approx 5 \times 10^{-2}$, whereas the reverse rate is only

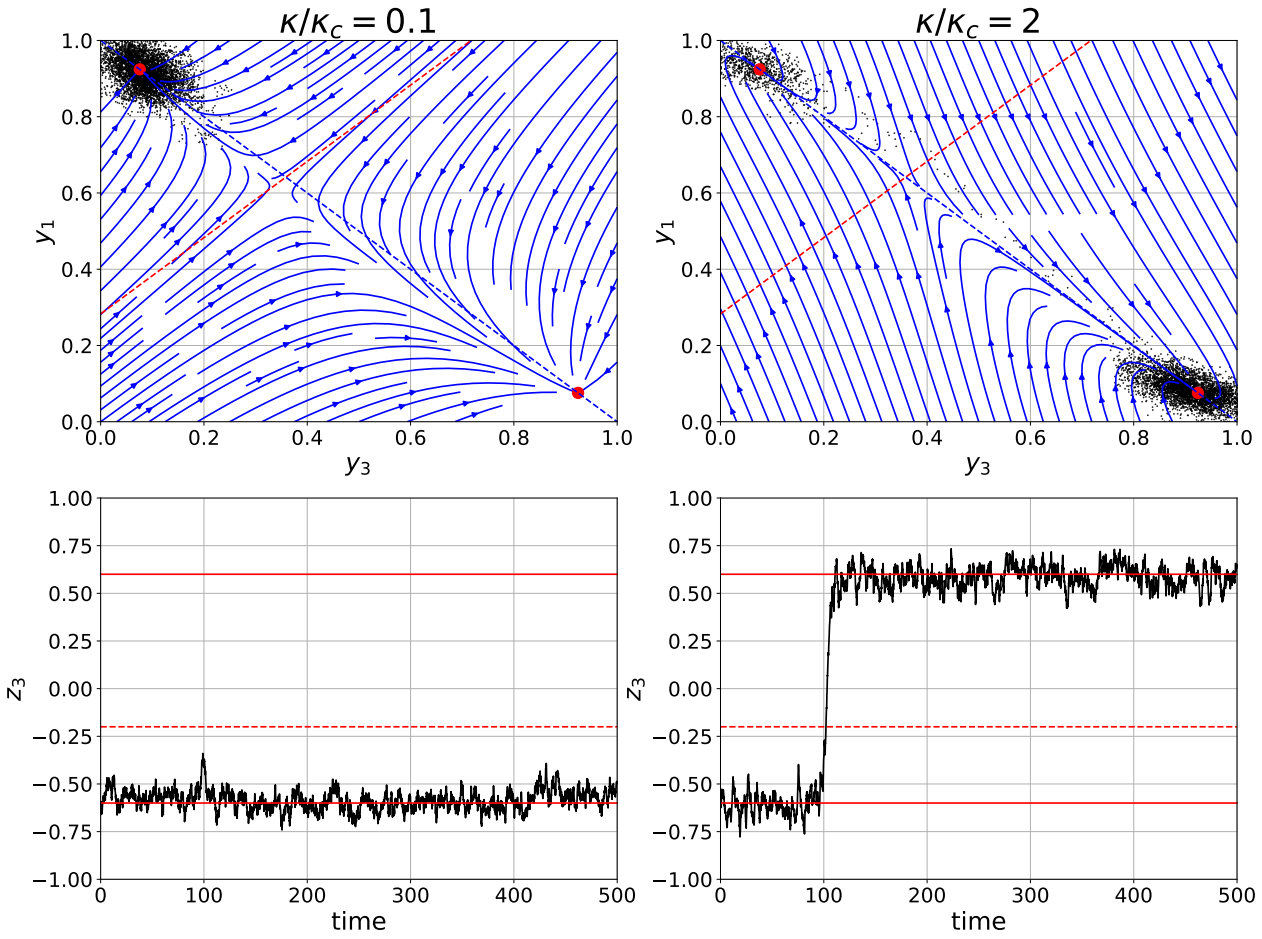

FIG. 3. Simulation of a nonlinear two-dimensional system described in the (z_1, z_3) by (98), with parameters $z_{3,0} = -0.2$, $z_{3,+} = 0.6$, $z_{3,-} = -0.6$ $\omega_1 = \omega_3 = 1$, $\delta = 0.001$, and $\kappa_c = 10$. The left panels correspond to $\kappa = \kappa_c/10$, while the right panels correspond to $\kappa = 2\kappa_c$.
Top panels: dynamics in phase space (y_1, y_3) (83), where the horizontal axis denotes the ratio of methylated site (y_3) and the vertical axis the ratio of unmethylated site (y_1). Red dots mark the stable equilibria, blue arrows indicate the force vector field, and the dashed red line the axis z_1 and the blue dashed line the axis z_3, which crosses each other at the unstable equilibrium.
Bottom panels: time series of the reaction variable (z_3). Continuous red lines mark the stable equilibria at $z_{3,\pm} = \pm 0.6$, and the dashed red line marks the unstable equilibrium at $z_{3,0} = -0.2$.
All simulations are performed over a time horizon $T = 500$ with integration step $\Delta t = 0.1$, corresponding to $N = 5000$ time steps.

$\Gamma_{z_{3,+} \to z_{3,-}} \approx 10^{-5}$. Thus, non-normality can explain the rapid transitions between states, but such transitions are not necessarily reversible due to the asymmetry of the potential landscape.
Conclusion. Non-normality thus reconciles bistability with rapid dynamics: DNA methylation can be both stable (supporting epigenetic memory) and fast-adapting (enabling minute-scale responses) through transient amplification of stochastic fluctuations.

F. Conclusion

We have shown how an existing nonlinear model of CpG dyads [11] can be extended with explicit stochasticity and analyzed through the lens of non-normality. This approach reveals how a purely deterministic bistable model, once augmented by a non-normal control parameter κ, can amplify thermal fluctuations and thereby accelerate transitions between unmethylated and methylated states without altering the system's spectral stability. In this way, non-normality provides a mechanistic explanation for the rapid DNA methylation dynamics observed experimentally [7], while preserving the underlying bistability that supports epigenetic memory.
Biological interpretation of κ. The parameter κ quantifies the strength of non-normal amplification in our reduced model. Biologically, it integrates the balance between DNA methyltransferases (DNMTs) and TET demethylases. DNMT3a and DNMT3b establish new methylation marks, DNMT1 maintains them during replication, while TET enzymes actively remove them via iterative oxidation of 5-methylcytosine. Thus, elevated

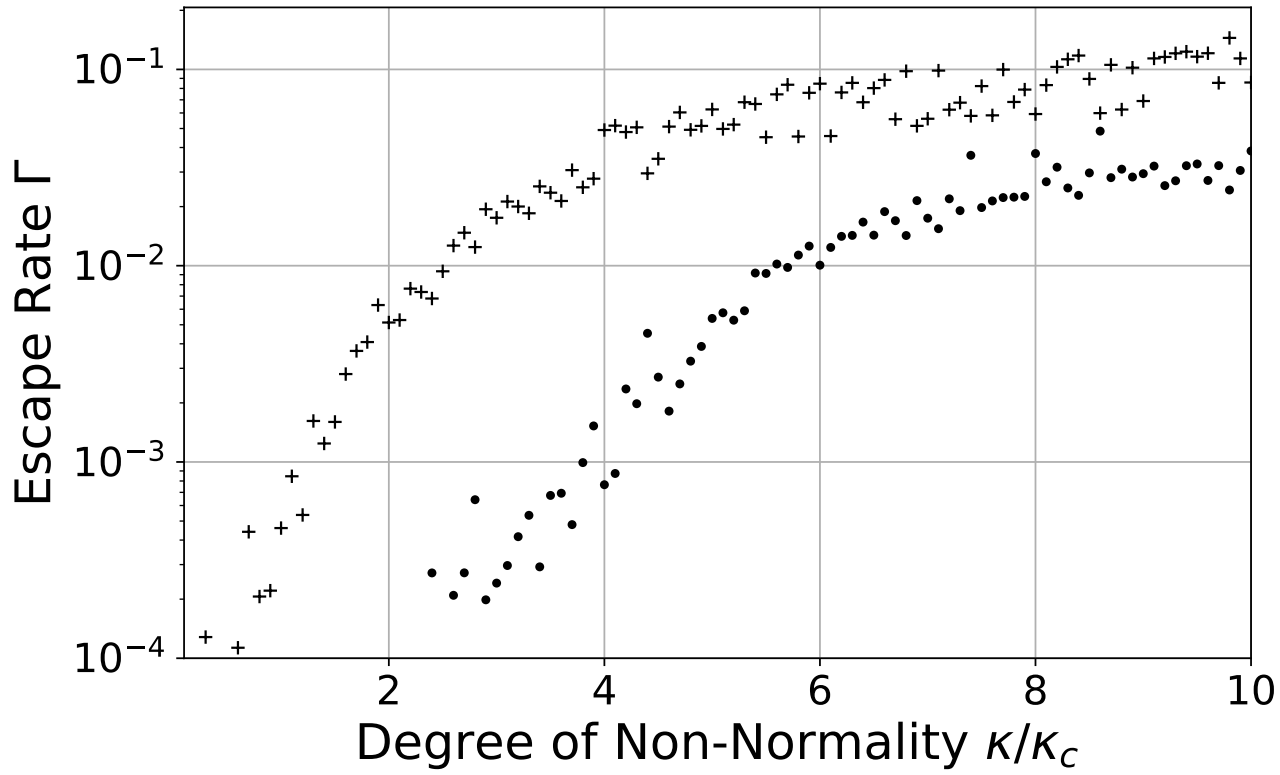

FIG. 4. Escape rate of the reaction variable z_3 as a function of κ/κ_c. Plain dots (".") denote transitions from $z_3 > z_{3,0}$ to $z_3 < z_{3,0}$, while crosses ("+") denote the reverse transitions. The dynamics follow (98) with parameters $z_{3,0} = -0.2$, $z_{3,+} = 0.6$, $z_{3,-} = -0.6$, $\omega_1 = \omega_3 = 1$, $\delta = 0.001$, and $\kappa_c = 10$. Simulations are performed for κ ranging from $\kappa_c/10$ to $10\kappa_c$, each run covering a total time $T = 10^5$ with integration step $\Delta t = 0.1$, corresponding to $N = 10^5$ sampled points. The escape rate is computed as $\Gamma = 1/\langle\tau\rangle$, where $\langle\tau\rangle$ is the mean first-passage time across the unstable saddle $z_{3,0}$.

DNMT activity or reduced TET activity can correspond to high κ, whereas the converse produces low κ.

Low-κ regimes. If $1 < \kappa < \kappa_c$, fluctuations are not strongly amplified, and fare from the criticality the system stays asymptotically stable. The only way for the system to transit between equilibrium, is to spectral criticality.

High-κ regimes. When $\kappa \gtrsim \kappa_c$, non-normality strongly renormalizes effective noise, enabling rapid switching. This regime can arise through:

- DNMT overexpression or TET downregulation: observed in several cancers [12, 13], leading to accelerated conversion of hemimethylated sites into fully methylated ones.
- Efficient maintenance methylation: when DNMT1 rapidly restores methylation after replication and demethylation processes are weak, as observed in certain adult tissues and tumor cell lines [13].
- TET hyperactivity or reduced DNMT expression: producing a net bias toward demethylation, as seen in promoters of constitutively hypomethylated genes [14, 15].
- Passive demethylation: inefficient DNMT1 activity, particularly during aging, leads to progressive loss of methylation across divisions [14].

The difference between the regime can be quantify by the asymmetry in the potential (98).

Closing. In summary, DNA methylation provides a compelling application of our extended non-variational Kramers framework. The degree of non-normality κ can, in principle, be inferred from empirical measurements of methylation state transitions. Evidence from both normal and pathological contexts suggests that methylation dynamics frequently operate in the high-κ regime, where transient amplification drives rapid state switching. By extending the model in [11] to include Gaussian noise and non-normal amplification, we reconcile bistability with fast epigenetic responses, providing a theoretical basis for the sudden methylation transitions observed in vivo [7].

V. OVERDAMPED KRAMER ESCAPE RATE

In this section, we introduce the mathematical framework used to derive the escape rate in the overdamped limit. We are borrowing from the derivation made by H.A. Kramer (1940) [16] of the escape rate of a particle in a one dimensional potential well in the overdamped limit.

We consider a system described by x, evolving in a potential $U(x)$ with a minimum at x_i and a potential barrier at x_f. Therefore, in the overdamped limit, we can write a one-dimensional Langevin equation as

$$\dot{x} = -U'(x) + \sqrt{2\delta}\eta(t). \tag{99}$$

For this problem, we know that the probability density function $P(x,t)$ satisfies the Fokker-Planck equation

$$\partial_t P = \partial_x \left[U'(x)P\right] + \delta\partial_x^2 P = -\partial_x J, \tag{100a}$$

$$\text{where } J(x,t) = -U'(x)P - \delta\partial_x P \tag{100b}$$

is the probability current. If the probability is constant and the current is equal to zero ($J(x,t) = 0$), the solution of the Fokker-Planck equation is given by the Boltzmann distribution i.e. $P(x) \sim e^{-U(x)/\delta}$.

To obtain the escape rate of the particle from the potential well, we search for an almost stationary solution of the Fokker-Planck equation i.e. $\partial_t P \approx 0$, which allows us to assume that the probability current is almost constant and uniform i.e. $J(x,t) = J$. This leads to

$$J = -U'(x)P - \delta\partial_x P = -\delta e^{-\frac{U(x)}{\delta}}\partial_x\left[e^{\frac{U(x)}{\delta}}P\right] \tag{101}$$

$$\Rightarrow \quad \partial_x\left[e^{\frac{U(x)}{\delta}}P\right] = \frac{J}{\delta}e^{\frac{U(x)}{\delta}}. \tag{102}$$

Integrating the last equation from the bottom of the potential well at x_i to a point x', even beyond the potential barrier at x_f, and assuming that the probability density is almost zero at x', the probability current is obtained from

$$\frac{J}{\delta}\int_{x_i}^{x'} e^{\frac{U(x)}{\delta}}\,\mathrm{d}x = e^{\frac{U(x')}{\delta}}P[x=x'] - e^{\frac{U(x_i)}{\delta}}P[x=x_i] \tag{103a}$$

$$\approx -e^{\frac{U(x_i)}{\delta}}P[x=x_i] \quad \text{since } P[x=x'] \approx 0, \tag{103b}$$

$$\Rightarrow \quad J \approx \delta\frac{P\left[x=x_i\right]e^{\frac{U(x_i)}{\delta}}}{\int_{x_i}^{x'} e^{\frac{U(x)}{\delta}}dx}. \tag{104}$$

The escape rate Γ is given by the probability current per unit of time, conditional to having the particle in the well. Denoting the probability that the particle is in the well as p_0, the probability current is $J = p_0\Gamma$. Under the hypothesis that the barrier is high enough, the probability that the particle is in the well can be approximated by

$$p_0 = \int_{x_i-\delta}^{x_i+\delta} P(x)\,\mathrm{d}x \tag{105}$$

$$\approx P[x=x_i]\int_{x_i-\delta}^{x_i+\delta} e^{-\frac{1}{\delta}(U(x)-U(x_i))}\,\mathrm{d}x \tag{106}$$

$$\approx P[x=x_i]\int_{x_i-\delta}^{x_i+\delta} e^{-\frac{1}{2\delta}U''(x_i)x^2}\,\mathrm{d}x \tag{107}$$

$$\approx P[x=x_i]\int_{-\infty}^{+\infty} e^{-\frac{1}{2\delta}U''(x_i)(x-x_i)^2}\,\mathrm{d}x \tag{108}$$

$$\Rightarrow\ p_0 \approx P[x=x_i]\sqrt{\frac{2\pi\delta}{U''(x_i)}} \quad . \tag{109}$$

On the other hand, the integral in the denominator of the probability current (104) can be approximated by

$$\int_{x_i}^{x'} e^{\frac{1}{\delta}U(x)}\,\mathrm{d}x \approx e^{\frac{1}{\delta}U(x_f)}\int_{x_i}^{x'} e^{\frac{1}{2\delta}U''(x^*)(x-x_f)^2}\,\mathrm{d}x \tag{110}$$

$$\approx e^{\frac{1}{\delta}U(x_f)}\int_{-\infty}^{+\infty} e^{-\frac{1}{2\delta}|U''(x_f)|(x-x_f)^2}\,\mathrm{d}x \tag{111}$$

$$\approx \sqrt{\frac{2\pi\delta}{|U''(x^*)|}}e^{\frac{1}{2\delta}U(x_f)} \quad . \tag{112}$$

We thus obtain the escape rate as

$$\Gamma = \frac{1}{2\pi}\sqrt{U''(x_i)|U''(x_f)|}\;\; e^{-\frac{\Delta E}{2\delta}}, \tag{113}$$

where $\Delta E = U(x_f) - U(x_i)$ is the height of the potential barrier.

---

[1] J. X. Zhou, M. Aliyu, E. Aurell, and S. Huang, Quasi-potential landscape in complex multi-stable systems, Journal of the Royal Society Interface **9**, 3539 (2012).

[2] E. Glötzl and O. Richters, Helmholtz decomposition and potential functions for n-dimensional analytic vector fields, Journal of Mathematical Analysis and Applications **525**, 127138 (2023).

[3] V. Troude, S. Lera, K. Wu, and D. Sornette, Crises without tipping points: Pseudo-bifurcations from non-normal dynamics (2024), arXiv:2412.01833 [nlin.CD].

[4] V. Troude and D. Sornette, Unifying framework for amplification mechanisms: Criticality, resonance and non-normality (2025), arXiv:2506.01996 [nlin.CD].

[5] T. Biancalani, F. Jafarpour, and N. Goldenfeld, Giant amplification of noise in fluctuation-induced pattern formation, Physical Review Letters **118**, 018101 (2017).

[6] B. F. Farrell and P. J. Ioannou, Generalized stability theory. part i: Autonomous operators, Journal of the Atmospheric Sciences **53**, 2025 (1996).

[7] L. Busto-Moner, J. Morival, H. Ren, A. Fahim, Z. Reitz, T. L. Downing, and E. L. Read, Stochastic modeling reveals kinetic heterogeneity in post-replication DNA methylation, PLoS computational biology **16**, e1007195 (2020).

[8] T. Baubec, D. Colombo, C. Wirbelauer, J. Schmidt, L. Burger, A. Krebs, A. Akalin, and D. Schübeler, Genomic profiling of DNA methyltransferases reveals a role for dnmt3b in genic methylation, Nature **520**, 243 (2015).

[9] J. J. Day and J. D. Sweatt, DNA methylation and memory formation, Nature neuroscience **13**, 1319 (2010).

[10] M. Kim and J. Costello, DNA methylation: an epigenetic mark of cellular memory, Experimental & molecular medicine **49**, e322 (2017).

[11] L. Zagkos, M. Auley, J. Roberts, and N. Kavallaris, Mathematical models of DNA methylation dynamics: Implications for health and ageing, Journal of Theoretical Biology **462**, 184 (2019).

[12] M. Klutstein, D. Nejman, R. Greenfield, and H. Cedar, DNA methylation in cancer and aging, Cancer Research **76**, 3446 (2016).

[13] A. McGovern, B. Powell, and J. Chevassut, A dynamic multi-compartmental model of DNA methylation with demonstrable value in hematological malignancies, Journal of Theoretical Biology **310**, 14 (2012).

[14] Y. Li, Y. Liu, F. Strickland, and B. Richardson, Age-dependent decreases in DNA methyltransferase levels and low transmethylation micronutrient levels synergize to promote overexpression of genes implicated in autoimmunity and acute coronary syndromes, Experimental Gerontology **45**, 312 (2010).

[15] A. Hunter, P. Spechler, A. Cwanger, *et al.*, DNA methylation is associated with altered gene expression in amd, Investigative Ophthalmology and Visual Science **53**, 2089 (2012).

[16] H. A. Kramers, Brownian motion in a field of force and the diffusion model of chemical reactions, Physica **7**, 284 (1940).